# On the Low-Order Partial-Fraction Fitting of Dielectric Functions at Optical Wavelengths

Krzysztof A. Michalski, *Fellow, IEEE*

***Abstract*—Low-order partial-fraction (PF) fitting of optical dielectric functions from tabulated frequency data is investigated. Two rational function identification techniques are examined, viz., the Sanathanan–Koerner iteration and vector fitting, and it is found that these methods generate PF models of similar quality and both provide excellent starting solutions for further improvement by nonlinear optimizers. High-quality, wide-band PF models are obtained for several metals frequently encountered in plasmonic applications. These models are stable and well-suited for the finite-difference time-domain (FDTD) simulation of light interaction with nanostructures. An efficient FDTD updating scheme for PF media is also demonstrated.**

***Index Terms*—Curve fitting, dispersive media, FDTD methods, rational approximation, vector fitting.**

## I. Introduction

FOR dispersive media, the complex dielectric constant (or permittivity) $\epsilon$ is frequency dependent and is often referred to as the dielectric function, especially at optical wavelengths. A treasure trove of measured optical constants can be found in the literature [1]–[8] and online [9], [10]. For noble metals, the classical reference is Johnson and Christy (JC) [1] and the chapter by Lynch and Hunter [11] in Palik's handbook (PH) [7]. In electromagnetic simulations, it is often required that tabulated dielectric constant be interpolated across a wide frequency range [12]. Since the physics of the polarization of matter is well understood [13], phenomenological models have traditionally been used for that purpose. For example, Rakić *et al.* [14] used the Drude–Lorentz model to fit the dielectric functions of 11 metals at optical wavelengths, and these fits have been widely used and are available in MEEP [15].

In this work, we investigate the fitting of tabulated optical dielectric functions[1] with the partial fraction (PF) model

$$\epsilon(s) = e + \frac{d}{s} + \sum_{i=1}^{N} \frac{c_i}{s - p_i}, \quad s = j\omega \tag{1}$$

where $N$ is the model order, $e$ and $d$ are real parameters, and $p_i$ and $c_i$ are the poles (assumed to be simple) and residues, respectively, that are either real or come in complex-conjugate pairs. The constant term $e$ in (1) should, strictly speaking, be unity—as all polarization effects cease for $\omega \to \infty$, but we treat it as an adjustable parameter in the identification procedure. This extra degree of freedom often results in improved dielectric function models over finite frequency bands [16]. The second term in (1) represents the conduction effect so that $d = \sigma_0/\epsilon_0$, where $\sigma_0$ is the nominal conductivity [17]. This term can further combine with one of the real pole terms in the sum to form the Drude function, which is most suitable for metals [18]. For nonconductors this term may be omitted, in which case (1) simplifies to the model of Han *et al.* [19]. The complex-conjugate pole terms in (1) can represent both the Lorentz oscillators and the critical point (CP) functions [20]. The PF model (1) thus unifies in a simple form the dielectric dispersion models that have been used heretofore [17]–[19], [21]–[24]. Is also well suited for parameter identification from frequency-domain data, as well as for implementation in the finite-difference time-domain (FDTD) method [25].

The PF expansion (1) may be expressed in the rational fraction (RF) form

$$\epsilon(s) = \frac{P(s, \boldsymbol{a})}{sQ(s, \boldsymbol{b})} = \frac{\sum_{i=0}^{N+1} a_i s^i}{s \sum_{i=0}^{N} b_i s^i}, \quad s = j\omega \tag{2}$$

where $\boldsymbol{a}$ and $\boldsymbol{b}$ are vectors comprising the real polynomial coefficients $a_i$ and $b_i$, respectively, with $b_N = 1$. The RF model has traditionally been used in the identification of linear system transfer functions from frequency-domain data. The parameters of (1) can readily be obtained, once $a_i$ and $b_i$ have been found. A variant of (2), which does not include the static pole, was recently used by Han *et al.* [26].

Given a set of samples $\{s_k = j\omega_k, \hat{\epsilon}(s_k)\}_{k=1}^{M}$, the model (1) or (2) should match the data in a least-squares sense. The fitting error at the frequency $\omega_k$ is $E_k = \epsilon_k - \hat{\epsilon}_k$, with the notation $\epsilon_k \equiv \epsilon(s_k)$. The model parameters, which we arrange in a real vector $\boldsymbol{\theta}$, may be found by minimizing the cost function

$$\begin{aligned} C(\boldsymbol{\theta}) &= \sum_{k=1}^{M} \left[ W_k'^2 (\Re E_k)^2 + W_k''^2 (\Im E_k)^2 \right] \\ &= \begin{bmatrix} \boldsymbol{W}' \Re \boldsymbol{E} \\ \boldsymbol{W}'' \Im \boldsymbol{E} \end{bmatrix}^T \begin{bmatrix} \boldsymbol{W}' \Re \boldsymbol{E} \\ \boldsymbol{W}'' \Im \boldsymbol{E} \end{bmatrix} \equiv \boldsymbol{R}^T(\boldsymbol{\theta}) \boldsymbol{R}(\boldsymbol{\theta}) \end{aligned} \tag{3}$$

where $\boldsymbol{E}$ is a complex vector comprising the residuals $E_k$, $\boldsymbol{W}'$ and $\boldsymbol{W}''$ are real diagonal matrices comprising the weights $W_k'$ and $W_k''$ associated with the real and imaginary parts of the data, respectively, the superscript $T$ denotes a matrix transpose, and the symbols $\Re$ and $\Im$ denote real and imaginary parts, respectively. User-defined weights can often improve the fit quality. Since the variance of the measurements is usually not provided, it is reasonable to assume that the uncertainties are proportional to the magnitudes of the data values, and one may choose $W_k' = |\Re \hat{\epsilon}_k|^{-1}$ and $W_k'' = |\Im \hat{\epsilon}_k|^{-1}$, which is referred to as proportional weighting. With this weighting, which is most appropriate

Manuscript received February 24, 2013; revised August 06, 2013; accepted September 11, 2013. Date of publication September 16, 2013; date of current version November 25, 2013.

The author is with the Department of Electrical and Computer Engineering, Texas A&M University, College Station, TX 77843-3128 USA.

Digital Object Identifier 10.1109/TAP.2013.2282082

[1]Usually the refractive index $\tilde{n} = \sqrt{\epsilon} = n - j\kappa$, rather than $\epsilon = \epsilon' - j\epsilon''$, is tabulated. The dielectric function table is thus obtained as $\epsilon = \tilde{n}^2$. With the $e^{j\omega t}$ time convention assumed here, $\kappa > 0$ and $\epsilon'' > 0$ for passive media.

when the measurement errors in the real and imaginary parts are uncorrelated, relative, rather than absolute errors, are minimized.

The necessary condition for the minimum of (3) is that $dC/d\boldsymbol{\theta} = 0$, which leads to a set of nonlinear equations, because the unknown poles $p_i$ in (1), or the polynomial coefficients $b_i$ in (2), appear in the denominators of rational functions. Consequently, it is rather difficult to estimate the system parameters in a fast and reliable way. The *de facto* standard method for solving this nonlinear least-squares (NLS) problem is the Levenberg–Marquardt (LM) algorithm [27]. The user is often required to provide functions that compute the vector of residuals $\boldsymbol{R}(\boldsymbol{\theta})$ and the Jacobian matrix $\boldsymbol{J}(\boldsymbol{\theta}) = d\boldsymbol{R}/d\boldsymbol{\theta}$, as well as the starting parameter values. Although convergence to a global minimum is not guaranteed, successful applications to the dielectric function identification have been reported by Pernice *et al.* [22] (using the Fortran subroutine NL2SOL [28] from Netlib) and by Han *et al.* [19] (using the MATLAB function `lsqcurvefit`). Genetic algorithms and simulated annealing (SA) [29] are also suitable for this problem. The latter was pioneered in the present context by Rakić *et al.* [14] and used by Vial and Laroche [30] and Han *et al.* [26], among others. Although extremely time consuming, this method seeks the global minimum of the cost function. Still another class of identification methods replace the NLS problem with a sequence of linear least-squares (LLS) estimators [31]. These methods are comparatively simple and fast and do not require the initial guess of the solution.

The purpose of this paper is to derive accurate PF models (1) of optical dielectric functions from tabulated frequency-domain data, using simple LLS methods, which utilize only standard numerical linear algebra libraries. To this end, we have adapted two rational function identification techniques, which appear to be particularly well suited for this problem: 1) the Sanathanan–Koerner (SK) iteration [32], which is based on the RF form (2), and 2) vector fitting (VF) [33], which uses the PF form (1) directly. To the author's knowledge, neither has yet been applied to the identification of dielectric functions, although it has been recently suggested that these methods be used to provide the initial solution for subsequent optimization by SA [26]. We further improve (or "polish") the SK- and VF-generated models using an LM solver. Our focus is wideband, low-order PF models (with $N \leq 7$, say) that are stable in the time domain. We list the model parameters extracted for several metals frequently encountered in plasmonic applications. These models are particularly useful in FDTD simulations of light interaction with nanostructures. Hence, we also present a simple and efficient FDTD updating scheme for PF media and illustrate its application to compute the transmission spectrum of a silver nanolayer.

## II. Dielectric Function Identification

### A. Sanathanan–Koerner Iteration

We apply the SK [32] method in conjunction with the RF form (2). SK is an iterative procedure, in which the residuals $E_k$ in (3) are replaced by

$$E_k^{\mathrm{SK}} = \frac{s_k^{-1} P(s_k, \boldsymbol{a}^t) - \hat{\epsilon}_k Q(s_k, \boldsymbol{b}^t)}{Q(s_k, \boldsymbol{b}^{t-1})} \tag{4}$$

where the superscript $t$ is the iteration index. Since the denominator function is defined by the coefficients from the previous iteration, the cost function (3) becomes linear in the polynomial coefficients $\boldsymbol{a}$ and $\boldsymbol{b}$ so that the original NLS problem is replaced by a sequence of LLS problems. On the first iteration, the denominator in (4) is set to unity, hence no initial guess of the solution vector is required. In fact, the first iteration residuals are exactly those used by Levy [34] so that the SK iteration begins with the solution of the Levy curve fitting problem, which is also referred to as the *Cauchy problem* [35], [36]. Note that, in the Levy method, the residuals $E_k$ in (3) are multiplied by $Q(s_k, \boldsymbol{b})$, which tends to emphasize high-frequency errors. In the SK iteration, the denominator function in (4) plays the role of an adaptive weight that gradually removes this bias.

Setting the weighted residuals (4) to zero leads to the overdetermined linear system

$$\begin{bmatrix} \boldsymbol{W}' \Re \boldsymbol{A} \\ \boldsymbol{W}'' \Im \boldsymbol{A} \end{bmatrix} \begin{bmatrix} \boldsymbol{a} \\ \boldsymbol{b} \end{bmatrix} = \boldsymbol{0} \tag{5}$$

where $\boldsymbol{A}$ is a complex $M \times (2N+3)$ matrix, whose $k$th row is given as

$$\boldsymbol{A}_k = \Omega_k \left[ s_k^{-1}, \boldsymbol{v}_{kN}, -\hat{\epsilon}_k \boldsymbol{v}_{kN} \right] \tag{6}$$

with

$$\boldsymbol{v}_{kN} = \left[ 1, s_k, \cdots, s_k^N \right] \tag{7}$$

$$\Omega_k^t = \left( \boldsymbol{v}_{kN} \boldsymbol{b}^{t-1} \right)^{-1}, \quad \Omega_k^1 \equiv 1. \tag{8}$$

It is understood in the above that all quantities are evaluated at iteration $t$, with the superscript $t$ omitted where there is no danger of confusion. The system (5) is subject to the nontriviality constraint $b_N = 1$. Prior to the solution of (5), we improve the conditioning of the system matrix by column scaling, which balances the Euclidean norms of the matrix columns to unity [37]. These norms are saved and are later used to rescale the solution vector, but we omit these details here for brevity. We apply to (5) the mixed LS-TLS solution procedure [38], which exploits the fact that only a part of the system matrix is affected by errors in the tabulated data $\hat{\epsilon}_k$, viz., the part comprising the columns corresponding to the coefficients $\boldsymbol{b}$ of the denominator polynomial $Q(s)$. This method begins with the $\boldsymbol{QR}$ factorization[2] of the system matrix in (5), followed by partitioning of the upper-triangular matrix $\boldsymbol{R}$ into submatrices corresponding to the unknown vectors $\boldsymbol{a}$ and $\boldsymbol{b}$, as indicated below:

$$\boldsymbol{Q} \begin{bmatrix} \boldsymbol{R}_{11} & \boldsymbol{R}_{12} \\ \boldsymbol{0} & \boldsymbol{R}_{22} \end{bmatrix} \begin{bmatrix} \boldsymbol{a} \\ \boldsymbol{b} \end{bmatrix} = \boldsymbol{0}. \tag{9}$$

Note that $\boldsymbol{R}_{11}$ and $\boldsymbol{R}_{22}$ are also upper-triangular. The denominator coefficients $\boldsymbol{b}$ are then found from

$$\boldsymbol{R}_{22} \boldsymbol{b} = \boldsymbol{U} \boldsymbol{\Sigma} \boldsymbol{V}^T \boldsymbol{b} = \boldsymbol{0} \tag{10}$$

where the SVD of the matrix $\boldsymbol{R}_{22}$ is utilized. Here, $\boldsymbol{U}$ and $\boldsymbol{V}$ are matrices comprising the left and right singular vectors, respectively, and $\boldsymbol{\Sigma}$ is a diagonal matrix of singular values, held in a descending order of magnitude. The TLS solution of (10) is proportional to the right singular vector corresponding to the smallest singular value, hence we may choose $\boldsymbol{b} = \boldsymbol{V}_{N+1}$, where $\boldsymbol{V}_{N+1}$ is the last column of the matrix $\boldsymbol{V}$ [36]. At this

[2]The matrix $\boldsymbol{Q}$ must not be confused with the polynomial $Q(s)$.

stage, the poles $p_i$ of (1) are computed as eigenvalues of the $N \times N$ companion matrix of $Q(s)$, given as [39]

$$\begin{bmatrix} 0 & & & -b_0 \\ 1 & 0 & & -b_1 \\ & \ddots & \ddots & \vdots \\ & & 1 & -b_{N-1} \end{bmatrix} \tag{11}$$

where $\boldsymbol{b}$ is normalized so that $b_N = 1$. Since the polynomial coefficients are real, any complex poles will come in complex-conjugate pairs. If unstable poles occur, the signs of their real parts are changed to negative, thus flipping these poles back into the left half of the $s$-plane [33], and the coefficients $\boldsymbol{b}$ are reconstituted using the now stable roots [40]. The weights $\Omega_k^t$ in the matrix $\boldsymbol{A}$ are now updated, and the system (5) is solved again, resulting in an improved set of coefficients $\boldsymbol{b}$ (and poles $p_i$). These iterations are terminated when convergence is detected or a prescribed number of iterations is reached.

With the poles $p_i$ so determined, the other parameters of (1) may readily be found. First, the hitherto ignored coefficients $\boldsymbol{a}$ of the numerator polynomial $P(s)$ are computed by solving the triangular system

$$\boldsymbol{R}_{11}\boldsymbol{a} = -\boldsymbol{R}_{12}\boldsymbol{b}. \tag{12}$$

Then, the residues $c_i$ are found as

$$c_i = \frac{P(p_i)}{p_i Q'(p_i)} \tag{13}$$

where the prime denotes differentiation with respect to $s$, and the remaining two coefficients are obtained as $e = a_{N+1}$ (recall that $b_N = 1$) and $d = a_0/b_0$.

The SK method is not suitable for higher order model identification, due to the ill-conditioning associated with the Vandermonde-type matrices that arise in (5). This ill-conditioning can be remedied by switching from the monomial basis to orthogonal Forsythe polynomials, but the simplicity of the basic method would be lost [41]. Since our focus is low-order models, this change of basis was not essential here.

### *B. Vector Fitting Method*

Another iterative procedure, known as vector fitting (VF), was recently introduced by Gustavsen and Semlyen [33], who also made a MATLAB implementation freely available [42]. In VF, which invokes the coefficients of the PF model (1) directly, the residuals $E_k$ in (3) are replaced by

$$E_k^{\mathrm{VF}} = (\sigma\epsilon)^t(s_k) - \hat{\epsilon}_k \sigma^t(s_k) \tag{14}$$

where

$$\sigma^t(s) = \sum_{i=1}^{N} \frac{\tilde{c}_i^t}{s - p_i^{t-1}} + \tilde{d}^t \tag{15}$$

is an auxiliary function of the same order $N$ as (1), and

$$(\sigma\epsilon)^t(s) = e^t + \frac{d^t}{s} + \sum_{i=1}^{N} \frac{c_i^t}{s - p_i^{t-1}} \tag{16}$$

is a PF representation of the product $\sigma^t(s)\epsilon(s)$. Since only poles from the previous iteration are involved, (14) gives rise to a sequence of LLS estimators. Note that (16) postulates that $\sigma^t(s)\epsilon(s)$ has the same poles as $\sigma^t(s)$, apart from the static pole at the origin. This equation also implies that the zeros $z_i^t$ of $\sigma^t(s)$ cancel with the nonzero poles of the current rational approximation to $\epsilon(s)$. Hence, improved pole estimates can be obtained as zeros of $\sigma^t(s)$. If the latter is interpreted as the transfer function of a linear single-input and single-output (SISO) system, (15) fits the standard state-space framework [43], and it follows that $z_i^t$ may be found as the eigenvalues of the $N \times N$ matrix

$$\bar{\boldsymbol{A}} = \boldsymbol{\Lambda} - \tilde{d}^{-1}\boldsymbol{e}\tilde{\boldsymbol{c}}^T. \tag{17}$$

Here, $\boldsymbol{\Lambda} = \mathrm{diag}\{p_i\}$ is a diagonal matrix containing the current poles, $\boldsymbol{e}$ is a vector of ones, and $\tilde{\boldsymbol{c}}$ is a vector comprising the auxiliary residues $\tilde{c}_i$.

Setting the weighted residuals (14) to zero leads to the overdetermined linear system

$$\begin{bmatrix} \boldsymbol{W}'\Re\boldsymbol{A} \\ \boldsymbol{W}''\Im\boldsymbol{A} \end{bmatrix}\boldsymbol{\theta} = \boldsymbol{0} \tag{18}$$

where $\boldsymbol{\theta} = [c_1, \ldots, c_N, d, e, \tilde{c}_1, \ldots, \tilde{c}_N, \tilde{d}]^T$ and $\boldsymbol{A}$ is a complex $M \times (2N+3)$ matrix, whose $k$th row is given as

$$\boldsymbol{A}_k = \left[\boldsymbol{v}_{kN}, s_k^{-1}, 1, -\hat{\epsilon}_k\boldsymbol{v}_{kN}, -\hat{\epsilon}_k\right] \tag{19}$$

with

$$\boldsymbol{v}_{kN} = \left[(s_k - p_1)^{-1}, \cdots, (s_k - p_N)^{-1}\right]. \tag{20}$$

As stated, these equations are appropriate for real poles but should be modified for complex ones. Namely, if the poles $p_i$ and $p_{i+1}$ form a complex-conjugate pair, then the entries $\{(s_k - p_i)^{-1}, (s_k - p_{i+1})^{-1}\}$ in $\boldsymbol{v}_{k,N}$ should be replaced by

$$\left\{\left(\frac{1}{s_k - p_i} + \frac{1}{s_k - p_i^*}\right), \left(\frac{j}{s_k - p_i} - \frac{j}{s_k - p_i^*}\right)\right\}, \tag{21}$$

and the corresponding entries $\{c_i, c_{i+1}\}$ and $\{\tilde{c}_i, \tilde{c}_{i+1}\}$ in $\boldsymbol{\theta}^T$ should be replaced by $\{c_i', c_i''\}$ and $\{\tilde{c}_i', \tilde{c}_i''\}$ [33]. Note that we use primes and double-primes to denote the real and imaginary parts of a complex number. Although the LS-TLS method can also be applied to solve (18), it has been reported [44] that the so-called relaxed VF [45], which imposes the nontriviality constraint

$$\left[\frac{1}{M}\sum_{k=1}^{M}\Re\boldsymbol{v}_{kN}, 1\right]\begin{bmatrix}\tilde{\boldsymbol{c}} \\ \tilde{d}\end{bmatrix} = 1, \tag{22}$$

has superior pole relocation properties. Here, $\boldsymbol{v}_{kN}$ and $\tilde{\boldsymbol{c}}$ should be modified to accommodate complex poles, as described above. This constraint, multiplied by the weight [45]

$$w = \sqrt{\sum_{k=1}^{M}\left[W_k'^2(\Re\hat{\epsilon}_k)^2 + W_k''^2(\Im\hat{\epsilon}_k)^2\right]} \tag{23}$$

is appended to (18), and the augmented system is solved by the $\boldsymbol{QR}$ factorization method with column scaling.

VF is sensitive to the choice of the starting poles, which are usually set by heuristic procedures [33]. Here, we generate the initial poles $p_i$ by the Levy method, which is also the first step in SK. On subsequent iterations, these poles are set to the eigenvalues of the matrix $\bar{\boldsymbol{A}}$ given in (17), which can be reformulated, to ensure that the updated $p_i$ are either real or come out in perfect complex-conjugate pairs. Hence, if the current poles $p_i$ and $p_{i+1}$ form a complex-conjugate pair, the corresponding diagonal $2 \times 2$ block of the matrix $\boldsymbol{\Lambda}$ is modified as [33]

$$\begin{bmatrix} p_i & 0 \\ 0 & p_{i+1} \end{bmatrix} \rightarrow \begin{bmatrix} p_i' & p_i'' \\ -p_i'' & p_i' \end{bmatrix}, \tag{24}$$

and the corresponding entries in $\boldsymbol{e}^T$ and $\tilde{\boldsymbol{c}}^T$ are transformed as $\{1,1\} \rightarrow \{2,0\}$ and $\{\tilde{c}_i, \tilde{c}_{i+1}\} \rightarrow \{c_i', c_i''\}$, respectively. Note that the latter change has already been effected in the $\boldsymbol{\theta}$ above. If unstable poles arise, they are flipped as in the SK method. The iterations continue until convergence is detected or a predefined number of iterations is reached. A comparison of (14) and (4) indicates that VF may be considered a variant of the SK iteration, using partial fraction basis instead of monomials (which alleviates the ill-conditioning problem inherent in SK) and implicit re-weighting through pole relocation [44]. The conditioning of VF may further be improved by the use of orthonormal rational basis functions [46], but the implementation is somewhat complex.

The pole identification stage is followed by the residue identification step, which fits (1) directly to the tabulated data, using the known poles. This leads to the overdetermined system

$$\begin{bmatrix} \boldsymbol{W}' \Re \boldsymbol{A} \\ \boldsymbol{W}'' \Im \boldsymbol{A} \end{bmatrix} \boldsymbol{\theta} = \begin{bmatrix} \boldsymbol{W}' \Re \boldsymbol{b} \\ \boldsymbol{W}'' \Im \boldsymbol{b} \end{bmatrix} \tag{25}$$

where $\boldsymbol{\theta} = [c_1, \ldots, c_N, d, e]^T$, $\boldsymbol{b} = [\hat{\epsilon}_1, \ldots, \hat{\epsilon}_M]^T$, and $\boldsymbol{A}$ is a complex $M \times (N+2)$ matrix, whose $k$th row is given as

$$\boldsymbol{A}_k = \left[\boldsymbol{v}_{kN}, s_k^{-1}, 1\right]. \tag{26}$$

Here, $\boldsymbol{v}_{kN}$ is still given by (20), with the modification (21) for every complex-conjugate pole pair, and the corresponding changes are also made in $\boldsymbol{\theta}$, as explained earlier. The system (25) is also solved by $\boldsymbol{QR}$ factorization with column scaling.

## III. PF Model Extraction

It is essential for the success of the methods discussed here to utilize adequate linear algebra libraries in the solution of the LLS equations, which may be poorly conditioned. In this work, we have used the Fortran subroutine package LAPACK [47]. For the NLS solver, we have used the Fortran package N2GB, which is a variant of the earlier LM code NL2SOL [28] that admits user-specified parameter bounds. All computations were done in double precision.

As a basic test of the methods, we first apply SK and VF to synthetic data generated using the PF model (1) with the parameters listed in Table I. It is understood here that for every complex pole, its complex conjugate must also be included in the PF model (1). Further, it is assumed that $\omega$ is expressed

TABLE I
PF Model Parameters for Gold ($N = 5$)†

| | |
|---|---|
| $e = 1.1431$ | $d = 1.0622\text{E+3}$ |
| $p_1 = -7.1100\text{E-2}$ | $c_1 = -1.0622\text{E+3}$ |
| $p_2 = -2.9380\text{E-1} + j\,2.5480$ | $c_2 = 6.4274\text{E-1} - j\,2.2281\text{E-1}$ |
| $p_3 = -1.5504 + j\,2.7437$ | $c_3 = 7.5272 - j\,3.8615$ |

† Converted from the Vial *et al.* [24] Drude+2CP fit of JC data.

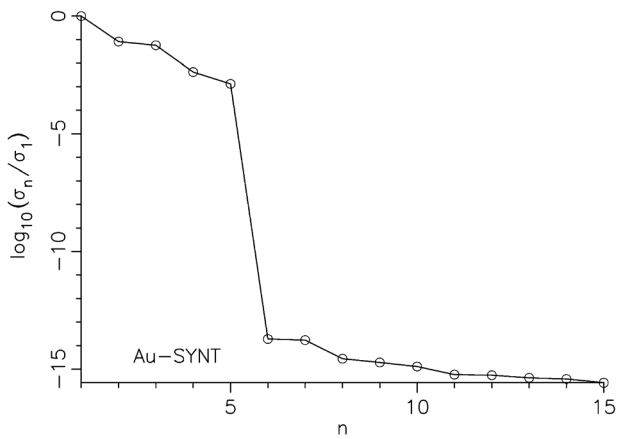


Fig. 1. Distribution of singular values when fitting synthetic Au data.

in electronvolts (eV).[3] The parameters listed correspond to the Drude+2CP model (comprising one Drude and two CP terms) fit to the dielectric function of gold (Au) from JC, obtained recently by Vial *et al.* [24] using SA in the range $0.4 < \lambda < 1$ $\mu$m (here, $\lambda$ denotes the free-space wavelength). In this case, there is one real pole (which combines with the static pole to form the Drude function) and two complex-conjugate pole pairs so that the model order $N = 5$. We have generated the synthetic dielectric function data using this model with the frequency samples from JC, which cover the frequency range $0.64 < \omega < 6.6$ eV ($1.937 > \lambda > 0.188$ $\mu$m). Applying SK and VF with $N = 5$ to these data, we find that both methods reproduce the parameters of Table I exactly, which confirms that our algorithms are sound.

In Fig. 1, we show the distribution of the singular values obtained in (10) when SK is applied to the synthetic data using $N = 14$. Note the steep drop-off after the fifth eigenvalue, which indicates that the appropriate model order is $N = 5$—as expected, since this was the order of the model used to generate the synthetic data. When SK is applied to fit the actual, tabulated Au data from JC, the resulting distribution of singular values is shown in Fig. 2. No steep drop-off is observed in this case, which indicates that the minimum required model order cannot be automatically determined for the measured data contaminated by noise and implies that, theoretically at least, increasing $N$ will always result in a closer fit. In the examples that follow, we use for comparison purposes the proportional-weighted (relative) root-mean-square fitting error, denoted by $\varepsilon_{\mathrm{rms}}$. Unfortunately, it is found that, when the model order exceeds a certain number depending on the quality of the data, sometimes as low as $N = 10$, nonphysical wiggles and spikes appear in the dielectric function plots so that a low $\varepsilon_{\mathrm{rms}}$ alone

[3]The photon energy $E$ [eV] and the angular frequency $\omega$ [rad/s] are related by $E = \hbar\omega$, where $\hbar \approx 6.582119 \times 10^{-16}$ [eV · s] is the Planck constant.

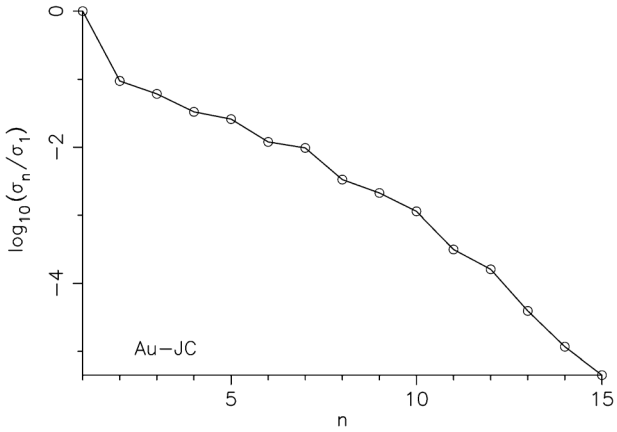


Fig. 2. Distribution of singular values when fitting tabulated Au data.

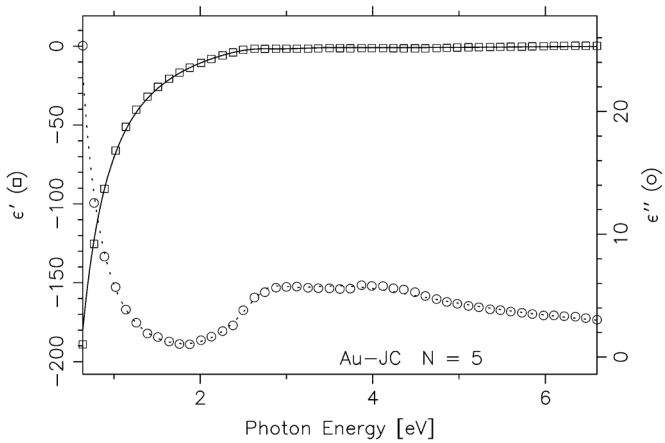


Fig. 3. PF ($N = 5$) fit for Au dielectric function from JC.

TABLE II
PF MODEL PARAMETERS FOR GOLD ($N = 5$)†

| | |
|---|---|
| $e = 1.3278$ | $d = 9.7831\text{E+2}$ |
| $p_1 = -7.8989\text{E-2}$ | $c_1 = -9.7790\text{E+2}$ |
| $p_2 = -3.8289\text{E-1}+j\,2.7826$ | $c_2 = -1.8920\text{E-1}-j\,1.0170$ |
| $p_3 = -1.2626 + j\,2.8881$ | $c_3 = 8.1464 - j\,2.3257$ |

† VF+LM fit of JC data ($\varepsilon_{\rm rms} = 4.719\text{E-2}$).

TABLE III
PF MODEL PARAMETERS FOR GOLD ($N = 7$)†

| | |
|---|---|
| $e = 1.0$ | $d = 9.6320\text{E+2}$ |
| $p_1 = -8.0129\text{E-2}$ | $c_1 = -9.6287\text{E+2}$ |
| $p_2 = -4.7259\text{E-1}+j\,2.7018$ | $c_2 = 7.2435\text{E-1}-j\,1.4189$ |
| $p_3 = -1.8003 + j\,2.7991$ | $c_3 = 9.7416 + j\,3.4040\text{E-2}$ |
| $p_4 = -7.4424\text{E-1}+j\,4.4474$ | $c_4 = -7.7534\text{E-1}-j\,4.2546\text{E-1}$ |

† SK+LM fit of JC data ($\varepsilon_{\rm rms} = 4.075\text{E-2}$).

TABLE IV
PF MODEL PARAMETERS FOR SILVER ($N = 6$)†

| | |
|---|---|
| $e = 1.0$ | $d = 2.5926\text{E+3}$ |
| $p_1 = -3.4089\text{E-2}$ | $c_1 = -2.5956\text{E+3}$ |
| $p_2 = -2.4860$ | $c_2 = 1.1961\text{E+1}$ |
| $p_3 = -2.5434\text{E-1}+j\,3.8737$ | $c_3 = 1.0284\text{E-1}+j\,3.999\text{E-1}$ |
| $p_4 = -8.9100\text{E-1}+j\,3.9425$ | $c_4 = 3.1782 - j\,5.5464\text{E-1}$ |

† SK+LM fit of JC data ($\varepsilon_{\rm rms} = 1.004\text{E-1}$).

TABLE V
PF MODEL PARAMETERS FOR SILVER ($N = 7$)†

| | |
|---|---|
| $e = 1.0$ | $d = 4.6904\text{E+4}$ |
| $p_1 = -1.7367\text{E-3}$ | $c_1 = -4.6896\text{E+4}$ |
| $p_2 = -9.6710\text{E-1}+j\,6.2681\text{E-1}$ | $c_2 = -1.0859 + j\,9.0177$ |
| $p_3 = -2.5138\text{E-1}+j\,3.9208$ | $c_3 = 2.8247\text{E-1}+j\,3.3354\text{E-1}$ |
| $p_4 = -1.0766 + j\,3.9631$ | $c_4 = 3.6945 - j\,7.1655\text{E-1}$ |

† SK+LM fit of JC data ($\varepsilon_{\rm rms} = 9.254\text{E-2}$).

does not guarantee a high-quality fit. The spikes are caused by spurious poles that are most likely to appear where there are gaps or outliers in the data. Although these poles may usually be identified by their excessively high $Q$-factors and heuristic procedures for their relocation have been proposed, the implementation is rather complex [48]. Therefore, visual inspection of the model-generated dielectric function plots is indispensable.[4] We thus generate models with increasing order $N$, until a high-quality fit is obtained. For the most important noble metals, gold and silver, we offer a choice of two models of different orders.

Regarding the relative performance of SK and VF, we have found that they produce similar results and are equally reliable. This may be due to the fact that, in our implementation, both methods begin with the same set of starting poles, produced by the Levy estimator. There may be some differences in the convergence behavior, but ultimately both methods generate models of similar quality, and both provide excellent starting points for further polishing by LM. Hence, in the examples presented here, we use either SK or VF, always selecting the method resulting in a smaller $\varepsilon_{\rm rms}$.

We first fit the PF model (1) to the JC-tabulated data for noble metals: gold (Au), silver (Ag), and copper (Cu). For Au, applying SK and VF with $N = 5$, and further polishing by LM, yields the PF model parameters in Table II. The listed $\epsilon_{\rm rms} = 4.719$ E-2 represents about a 2% improvement over the SK and VF results, which is typical for the examples presented here. The plot of the resulting PF fit of the dielectric function is shown in Fig. 3, where the tabulated data are indicated by symbols and separate scales are used for the real and imaginary parts. Raising the model order $N$ to 7 slightly reduces $\varepsilon_{\rm rms}$ to 4.075E-2, as indicated in Table III. Here and in some other cases that follow, we have imposed the constraint $e \geq 1$ in the LM step, since the optimal value of $e$ is often negative, which is nonphysical and may be undesirable. This restriction, however, tends to cause a deterioration in the fit quality, which is usually slight, but occasionally significant. Perhaps for this reason, some authors do not shy away from using $e < 0$ [20].

For Ag, applying SK with $N = 6$ and 7 yields the parameters in Tables IV and V, respectively, and the corresponding plot for $N = 6$ is given in Fig. 4. For Cu, applying VF and SK with $N = 6$ and 7 yields the parameters in Tables VI and VII, respectively, and the corresponding plot for $N = 6$ is given in Fig. 5.

Finally, we derive PF models for aluminum (Al) and chromium (Cr) using the tabulated data from PH. For consistency with the models obtained above, we limit the frequency

[4]In the words of one author [49], "The fitting is always a try-and-error activity, which requires a lot of human efforts and intuition." Fortunately, the algorithms presented here are fast so that trial PF models can be generated in seconds.

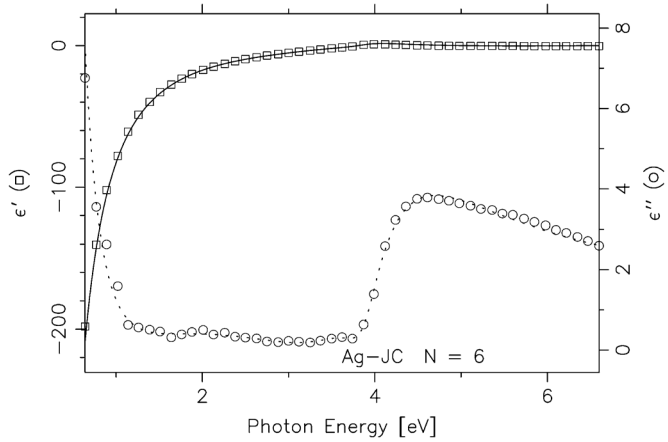


Fig. 4. PF ($N = 6$) fit for Ag dielectric function from JC.

TABLE VI
PF MODEL PARAMETERS FOR COPPER ($N = 6$)†

| | |
|---|---|
| $e = 1.0$ | $d = 6.7955\text{E+2}$ |
| $p_1 = -1.1821\text{E-1}$ | $c_1 = -6.8430\text{E+2}$ |
| $p_2 = -2.1356$ | $c_2 = 2.1042\text{E+1}$ |
| $p_3 = -3.0691\text{E-1}+j\,2.1325$ | $c_3 = 1.4822 + j\,2.1773\text{E-1}$ |
| $p_4 = -8.9676\text{E-1}+j\,5.3425$ | $c_4 = -1.0012 - j\,1.2254$ |

† VF+LM fit of JC data ($\varepsilon_{\text{rms}} = 3.230\text{E-2}$).

TABLE VII
PF MODEL PARAMETERS FOR COPPER ($N = 7$)†

| | |
|---|---|
| $e = 1.7665$ | $d = 7.4394\text{E+2}$ |
| $p_1 = -1.0616\text{E-1}$ | $c_1 = -7.4532\text{E+2}$ |
| $p_2 = -2.5740\text{E-1}+j\,2.1233$ | $c_2 = 1.0694 + j\,1.5767\text{E-1}$ |
| $p_3 = -2.1296 + j\,2.6916$ | $c_3 = 2.6922 - j\,9.6133$ |
| $p_4 = -8.3075\text{E-1}+j\,4.8844$ | $c_4 = 6.6689\text{E-1}-j\,1.4793$ |

† SK+LM fit of JC data ($\varepsilon_{\text{rms}} = 2.828\text{E-2}$).

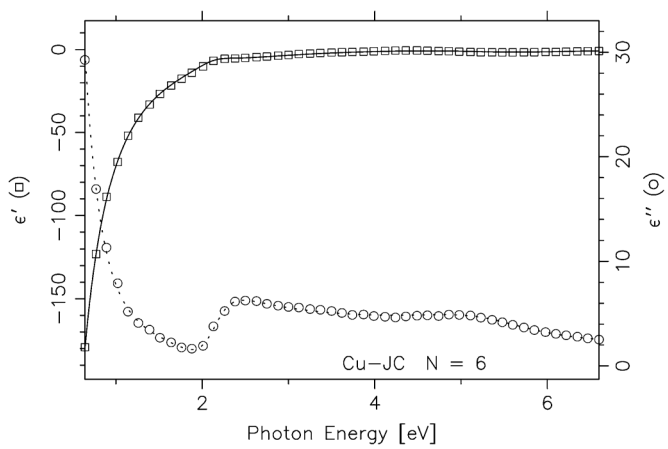


Fig. 5. PF ($N = 6$) fit for Cu dielectric function from JC.

range to that available in the JC tables. For Al, applying VF with $N = 5$ yields the parameters presented in Table VIII, and the corresponding plot is given in Fig. 6. For Cr, applying VF with $N = 7$ yields the parameters in Table IX, and the corresponding plot is given in Fig. 7.

TABLE VIII
PF MODEL PARAMETERS FOR ALUMINUM ($N = 5$)†

| | |
|---|---|
| $e = 1.0$ | $d = 1.3186\text{E+3}$ |
| $p_1 = -1.4661\text{E-1}$ | $c_1 = -1.3541\text{E+3}$ |
| $p_2 = -9.2093\text{E-1}+j\,7.4420\text{E-1}$ | $c_2 = 1.3445\text{E+1}-j\,3.7366\text{E+1}$ |
| $p_3 = -2.0507\text{E-1}+j\,1.4871$ | $c_3 = 4.1114 - j\,5.8421$ |

† VF+LM fit of PH data ($\varepsilon_{\text{rms}} = 1.387\text{E-2}$).

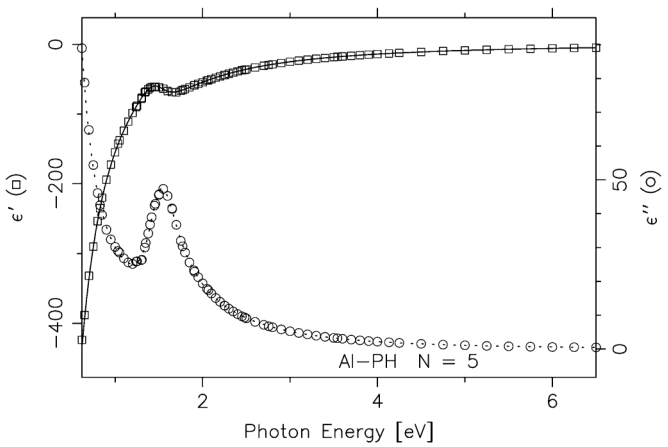


Fig. 6. PF ($N = 5$) fit for Al dielectric function from PH.

TABLE IX
PF MODEL PARAMETERS FOR CHROMIUM ($N = 7$)†

| | |
|---|---|
| $e = 2.1508$ | $d = 1.7292\text{E+2}$ |
| $p_1 = -1.4642\text{E-1}$ | $c_1 = -1.6340\text{E+2}$ |
| $p_2 = -1.8013 + j\,1.1172$ | $c_2 = -7.1487 - j\,8.8557\text{E+1}$ |
| $p_3 = -3.3664\text{E-1}+j\,2.6614$ | $c_3 = -1.8454 + j\,1.1286\text{E-1}$ |
| $p_4 = -1.1450 + j\,5.4642$ | $c_4 = 2.2579 - j\,1.0288$ |

† VF+LM fit of PH data ($\varepsilon_{\text{rms}} = 2.091\text{E-2}$).

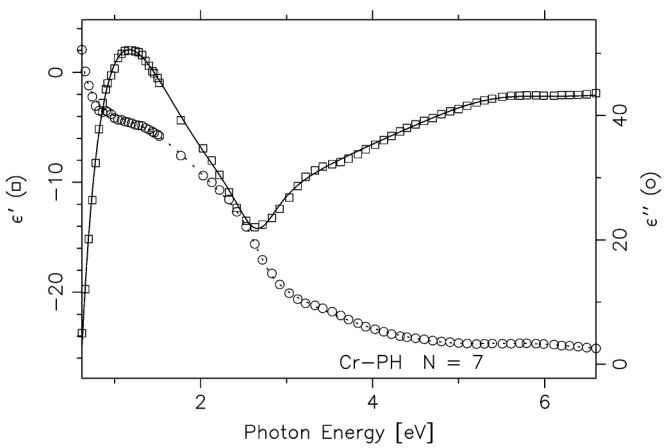


Fig. 7. PF ($N = 7$) fit for Cr dielectric function from PH.

## IV. FDTD MODELING OF PF MEDIA

In the FDTD method, the Maxwell's equations are discretized using central differences for both space and time derivatives, with the electric and magnetic fields, $\boldsymbol{E}$ and $\boldsymbol{H}$, respectively, evaluated at time instants shifted by a half of the time step $\Delta t$ [25]. Only the temporal discretization is addressed here, using the superscript $n$ to indicate fields evaluated at $t = n\Delta t$. To incorporate dispersive media characterized by the PF model (1)

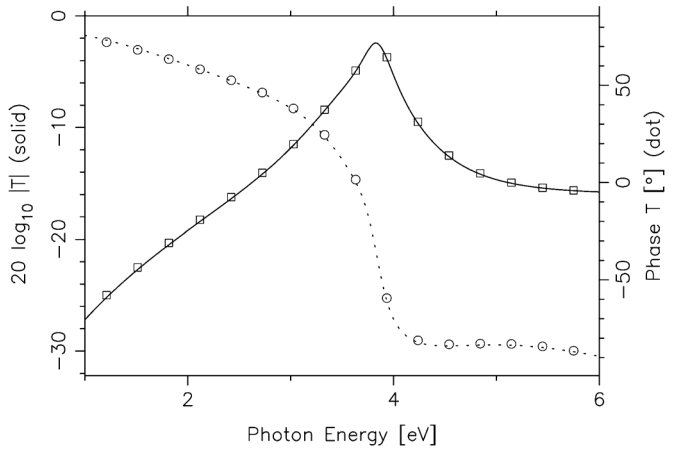


Fig. 8. Transmission coefficient of a 50-nm-thick Ag slab computed by the FDTD method using the PF model of Table IV (symbols) is compared with the exact result (lines).

into the FDTD framework, we have adopted the trapezoidal recursive convolution (TRC) method [50], which is comparable in terms of efficiency and ease of implementation to the auxiliary differential equation method [51] used by Han *et al.* [19] and Han *et al.* [26]. TRC was also recently applied to Drude-CP media by Shibayama *et al.* [52]. For PF media, the resulting FDTD updating equations are as follows:

$$\boldsymbol{E}^{n+1} = \frac{A^-}{A^+}\boldsymbol{E}^n + \frac{c\Delta t}{A^+}(\boldsymbol{\nabla}\times\boldsymbol{H})^{n+1/2} + \frac{1}{A^+}\sum_i \Re\Psi_i^n \tag{27}$$

$$\Psi_i^{n+1} = \frac{\boldsymbol{E}^{n+1}+\boldsymbol{E}^n}{2}\Delta\chi_i^0 + e^{p_i\Delta t}\Psi_i^n \tag{28}$$

where

$$A^{\mp} = e \mp \frac{d\Delta t}{2} \mp \frac{1}{2}\sum_i \Re\chi_i^0 \tag{29}$$

$$\chi_i^0 = -\frac{\xi_i c_i}{p_i}(1-e^{p_i\Delta t}), \quad \Delta\chi_i^0 = \chi_i^0(1-e^{p_i\Delta t}). \tag{30}$$

In the above, $\boldsymbol{H}$ stands for $\eta_0\boldsymbol{H}$, where $\eta_0 = \sqrt{\mu_0/\epsilon_0}$ is the intrinsic impedance of free space, and $c = 1/\sqrt{\mu_0\epsilon_0}$ is the speed of light. The summation index $i$ goes over the poles $p_i$ in (1), including only one pole per complex-conjugate pair, with $\xi_i = 1$ or 2, depending on whether $p_i$ is real or complex, respectively. For brevity, we have omitted the updating equation for $\boldsymbol{H}^{n+3/2}$, which is standard [25].

To illustrate the utility of the PF models developed here, we have computed the transmission spectrum of light through a 50-nm-thick Ag layer suspended in air using the FDTD method and FFT. The dielectric function of Ag was modeled using the parameters listed in Table IV, which were derived by fitting the data tabulated in JC. We have also solved the same problem by the analytical (exact) frequency-domain method [53]. The transmission coefficient spectra obtained by the two methods are compared in Fig. 8, and excellent agreement is observed. Results of similar quality are obtained for the other PF models presented here.

## V. Conclusion

We have investigated the application of two rational function identification methods, viz., the Sanathanan–Koerner (SK) iteration and vector fitting (VF), to the development of partial-fraction (PF) models of dielectric functions from tabulated data at optical wavelengths, with emphasis on low-order, wide-band models that are stable in the time domain. SK and VF are comparatively simple and are easily implemented using only standard numerical linear algebra libraries. We have found that, although there may be some differences in their convergence behavior, both methods generate models of similar quality and both provide excellent starting points for further polishing by nonlinear optimizers. We have also found that proportional weighting significantly improves the fit quality for the metals considered here. Further, we have found that the optimal model order cannot be determined for actual data contaminated by noise so that the fit accuracy generally improves with the increasing order. However, this improvement is soon arrested by the appearance of spurious poles, which cause nonphysical spikes in the dielectric function plots. An inspection of these plots is thus an indispensable part of the fitting process, but, fortunately, the algorithms presented here are fast so that trial PF models can be generated in seconds. We have listed the obtained PF model parameters for several metals frequently encountered in plasmonic applications. These models are stable and well suited for use in the FDTD simulation of light interaction with nanostructures. To demonstrate this, we have derived a simple FDTD updating scheme for PF media and applied it to compute the transmission spectrum of a silver nanolayer.

## References

[1] P. B. Johnson and R. W. Christy, "Optical constants of noble metals," *Phys. Rev. B*, vol. 6, no. 12, pp. 4370–4379, 1972.

[2] P. B. Johnson and R. W. Christy, "Optical constants of transition metals: Ti, V, Cr, Mn, Fe, Co, Ni, Pd," *Phys. Rev. B*, vol. 9, no. 12, pp. 5056–5070, 1974.

[3] D. E. Aspnes and A. A. Studna, "Dielectric functions and optical parameters of Si, Ge, GaP, GaAs, GaSb, InP, InAs, InSb from 1.5 to 6.0 eV," *Phys. Rev. B*, vol. 27, no. 2, pp. 985–1009, 1983.

[4] M. A. Ordal, L. L. Long, R. J. Bell, S. E. Bell, R. R. Bell, R. W. Alexander, and C. A. Ward, "Optical properties of the metals Al, Co, Cu, Au, Fe, Pb, Ni, Pd, Pt, Ag, Ti, W in the infrared and far infrared," *Appl. Opt.*, vol. 22, no. 7, pp. 1099–1119, 1983.

[5] M. A. Green and M. Keevers, "Optical properties of intrinsic silicon at 300 K," *Progr. Photovol.*, vol. 3, pp. 189–192, 1995.

[6] A. D. Rakić, "Algorithm for the determination of intrinsic optical constants of metal films: Application to aluminum," *Appl. Opt.*, vol. 34, no. 22, pp. 4755–4767, 1995.

[7] *Handbook of Optical Constants of Solids*, E. D. Palik, Ed. San Diego, CA, USA: Academic, 1998.

[8] N. P. Blanchard, C. Smith, D. S. Martin, D. J. Hayton, T. E. Jenkins, and P. Weightman, "High-resolution measurements of the bulk dielectric constants of single crystal gold with application to reflection anisotropy spectroscopy," *Phys. Stat. Sol. C*, vol. 0, no. 8, pp. 2931–2937, 2003.

[9] Refractive Index Database [Online]. Available: http://refractiveindex.info

[10] Refractive Index Database [Online]. Available: http://www.filmetrics.com/refractive-index-database

[11] D. W. Lynch and W. R. Hunter, "Comments on the optical constants of metals and an introduction to the data for several metals," in *Handbook of Optical Constants of Solids*, E. D. Palik, Ed. San Diego, CA, USA: Academic, 1998, pp. 275–316.

[12] A. S. McLeod, P. J. Schuck, and J. B. Nelson, "Finite time domain studies of plasmmonic nano-structures across wide frequency ranges," in *Proc. Conf. Lasers Electro-Optics (CLEO) Quantum Electron. Laser Sci.(QELS)*, San Jose, CA, USA, May 2010, pp. JThE31-1–JThE31-2.

[13] C. F. Bohren and D. R. Huffman, *Absorption and Scattering of Light by Small Particles*. New York, NY, USA: Wiley, 1983.

[14] A. D. Rakić, A. B. Djurišić, J. M. Elazar, and M. L. Majewski, "Optical properties of metallic films for vertical-cavity optoelectronic devices," *Appl. Opt.*, vol. 37, no. 22, pp. 5271–5283, 1998.
[15] A. F. Oskooi, D. Roundy, M. Ibanescu, P. Bermel, J. D. Joannopoulos, and S. G. Johnson, "MEEP: A flexible free-software package for electromagnetic simulations for FDTD method," *Comput. Phys. Commun.*, vol. 181, no. 3, pp. 687–702, 2010.
[16] A. Vial and T. Laroche, "Comparison of gold and silver dispersion laws suitable for FDTD simulations," *Appl. Phys. B*, vol. 93, pp. 139–143, 2008.
[17] F. Hao and P. Nordlander, "Efficient dielectric function for FDTD simulation of the optical properties of silver and gold nanoparticles," *Chem. Phys. Lett.*, vol. 446, pp. 115–118, 2007.
[18] T. Lee and S. K. Gray, "Subwavelength light bending by metal slit structures," *Opt. Exp.*, vol. 13, no. 24, pp. 9652–9659, 2005.
[19] M. Han, R. W. Dutton, and S. Fan, "Model dispersive media in finite-difference time-domain method with complex-conjugate pole-residue pairs," *IEEE Microw. Wireless Compon. Lett.*, vol. 16, pp. 119–121, Mar. 2006.
[20] J. Leng, J. Opsal, H. Chu, M. Senko, and D. E. Aspnes, "Analytic representations of the dielectric functions of materials for device and structural modeling," *Thin Solid Films*, vol. 313–314, pp. 132–136, 1998.
[21] P. G. Etchegoin, E. C. Le Ru, and M. Meyer, "An analytic model for the optical properties of gold," *J. Chem. Phys.*, vol. 125, pp. 164 705-1–164 705-3, 2006.
[22] W. H. P. Pernice, F. P. Payne, and D. F. G. Gallagher, "An FDTD method for the simulation of dispersive metallic structures," *Opt. Quantum Electron.*, vol. 38, pp. 843–856, 2006.
[23] S. G. Rodrigo, F. J. García-Vidal, and L. Martín-Moreno, "Influence of material properties on extraordinary optical transmission through hole arrays," *Phys. Rev. B*, vol. 77, pp. 075 401-1–075 401-8, 2008.
[24] A. Vial, T. Laroche, M. Dridi, and L. Le Cunff, "A new model of dispersion for metals leading to a more accurate modeling of plasmonic structures using the FDTD method," *Appl. Phys. A*, vol. 103, pp. 849–853, 2011.
[25] A. Taflove and S. C. Hagness, *Computational Electrodynamics: The Finite-Difference Time-Domain Method*. Norwood, MA, USA: Artech House, 2005.
[26] L. Han, D. Zhou, K. Li, X. Li, and W. Huang, "A rational-fraction dispersive model for efficient simulation of dispersive material in FDTD method," *J. Lightw. Technol.*, vol. 30, pp. 2216–2225, Jul. 2012.
[27] J. J. Moré, "The Levenberg-Marquardt algorithm: Implementation and theory," in *Lecture Notes in Mathemeatics*, G. A. Watson, Ed. Berlin, Germany: Springer, 1978, vol. 630, pp. 105–116.
[28] J. E. Dennis, D. M. Gay, and R. E. Welsch, "An adaptive nonlinear least-squares algorithm," *ACM Trans. Math. Softw.*, vol. 7, no. 3, pp. 348–368, 1981.
[29] H. Schhwefel, *Evolution and Optimum Seeking*. New York, NY, USA: Wiley, 1995.
[30] A. Vial and T. Laroche, "Description of dispersion properties of metals by means of the critical points model and application to the study of resonant structures using the FDTD method," *J. Phys. D, Appl. Phys.*, vol. 40, pp. 7152–7158, 2007.
[31] R. Pintelon, P. Guillaume, Y. Rolain, J. Schoukens, and H. Van Hamme, "Parametric identification of transfer functions in the frequency domain-A survey," *IEEE Trans. Autom. Control*, vol. 39, pp. 2245–2260, Nov. 1994.
[32] C. K. Sanathanan and J. Koerner, "Transfer function synthesis as a ratio of two complex polynomials," *IEEE Trans. Autom. Control*, vol. AC-8, pp. 56–58, Jan. 1963.
[33] B. Gustavsen and A. Semlyen, "Rational approximation of frequency domain responses by vector fitting," *IEEE Trans. Power Del.*, vol. 14, pp. 1052–1061, Jul. 1999.
[34] E. C. Levy, "Complex-curve fitting," *IEEE Trans. Autom. Control*, vol. AC-4, pp. 37–43, May 1959.
[35] J. Meinguet, "On the solubility of the Cauchy interpolation problem," in *Approximation Theory*, A. Talbot, Ed. London, U.K.: Academic, 1970, pp. 137–162.
[36] R. S. Adve, T. K. Sarkar, S. M. Rao, E. K. Miller, and D. R. Pflug, "Application of the Cauchy method for extrapolating/interpolating narrow-band system responses," *IEEE Trans. Microw. Theory Technol.*, vol. 45, pp. 837–845, May 1997.
[37] A. O. Soysal and A. Semlyen, "Practical transfer function estimation and its application to wide frequency range representation of transformers," *IEEE Trans. Power Del.*, vol. 8, pp. 1626–1637, Jul. 1993.
[38] S. Van Huffel and J. Vanderwalle, *The Total Least Squares Problem, Computational Aspects and Analysis*. Philadelphia, PA, USA: SIAM, 1991.
[39] A. Edelman and H. Murakami, "Polynomial roots from companion matrix eigenvalues," *Math. Comput.*, vol. 64, no. 210, pp. 763–776, 1995.
[40] O. González, J. A. Pereda, A. Herrera, A. Grande, and Á. Vegas, "Combining the FDTD method and rational-fitting techniques for modeling active devices characterized by measured S-parameters," *IEEE Microw. Wireless Compon. Lett.*, vol. 17, pp. 477–479, July 2007.
[41] M. H. Richardson and D. L. Formenti, "Parameter estimation from frequency response measurements using rational fraction polynomials," in *Proc. 1st Int. Modal Anal. Conf.*, Orlando, FL, USA, Nov. 1982, pp. 167–182.
[42] The Vector Fitting Web Site [Online]. Available: http://www.sintef.no/Projectweb/VECTFIT/
[43] I. Kaufman, "On poles and zeros of linear systems," *IEEE Trans. Circuit Theory*, vol. CT-20, pp. 93–101, Mar. 1973.
[44] D. Deschrijver, B. Gustavsen, and T. Dhaene, "Advancements in iterative methods for rational approximation in the frequency domain," *IEEE Trans. Power Del.*, vol. 22, pp. 1633–1642, Jul. 2007.
[45] B. Gustavsen, "Improving the pole relocating properties of vector fitting," *IEEE Trans. Power Del.*, vol. 21, pp. 1587–1592, Jul. 2006.
[46] D. Deschrijver, B. Haegeman, and T. Dhaene, "Orthonormal vector fitting: A robust macromodeling tool for rational approximation of frequency domain responses," *IEEE Trans. Adv. Packag.*, vol. 30, pp. 216–225, May 2007.
[47] E. Anderson, Z. Bai, C. Bischof, S. Blackford, J. Demmel, J. Dongarra, J. Du Croz, A. Greenbaum, S. Hammarling, A. McKenney, and D. Sorensen, *LAPACK User's Guide*, 3rd ed. Philadelphia, PA, USA: SIAM, 1999.
[48] S. Grivet-Talocia and M. Bandinu, "Improving the convergence of vector fitting for equivalent circuit extraction from noisy frequency responses," *IEEE Trans. Electromagn. Compat.*, vol. 48, pp. 104–120, Feb. 2006.
[49] A. Kuzmenko, "Guide to RefFIT software to fit optical spectra," [Online]. Available: http://optics.unige.ch/alexey/reffit.html
[50] R. Siushansian and J. LoVetri, "Efficient evaluation of convolution integrals arising in FDTD formulations of electromagnetic dispersive media," *J. Electramagn. Waves Appl.*, vol. 11, pp. 101–117, 1997.
[51] M. Okoniewski, M. Mrozowski, and M. A. Stuchly, "Simple treatment of multi-term dispersion in FDTD," *IEEE Microw. Guided Wave Lett.*, vol. 7, pp. 121–123, May 1997.
[52] J. Shibayama, K. Watanabe, R. Ando, J. Yamaguchi, and H. Nakano, "Frequency-dependent formulations of a Drude-critical points model for explicit and implicit FDTD methods using the trapezoidal RC technique," *IEICE Trans. Electron.*, vol. E95-C, no. 4, pp. 725–732, 2012.
[53] K. A. Michalski, "Electromagnetic field computation in planar multilayers," in *Encyclopedia of RF and Microwave Engineering*, K. Chang, Ed. Hoboken, NJ, USA: Wiley-Interscience, 2005, vol. 2, pp. 1163–1190.

**Krzysztof A. Michalski** (S'78–M'81–SM'88–F'01) received the M.S. degree from the Wrocław Technological University, Poland, in 1974 and the Ph.D. degree from the University of Kentucky, Lexington, in 1981, both in electrical engineering.

From 1982 to 1986, he was with the University of Mississippi, and since 1987 he has been with Texas A&M University, College Station, TX, USA. He also held visiting professorships with Ecole Polytechnique Fédérale de Lausanne, Université de Nice—Sophia Antipolis, Universitat Politecnica de Catalunya, and Technische Universität München, and served as Visiting Scientist with Sandia Laboratories and the National Institute of Standards and Technology. His research interests are in electromagnetic theory and computational electromagnetics, with emphasis on Green function methods and layered media.